Bioorg. Med. Chem. 67 (2022) 116814

Contents lists available at ScienceDirect

Bioorganic & Medicinal Chemistry

journal homepage: www.elsevier.com/locate/bmc

Dinuclear silver and gold bisNHC complexes as drug candidates for cancer therapy

Mireia Quintana [a,1], Alba Rodriguez-Rius [a,1], Alba Vellé [b], Sonia Vives [a], Pablo J. Sanz Miguel [b,*], Gemma Triola [a,*]

[a] Departamento de Química Biológica, Instituto de Química Avanzada de Cataluña (IQAC), CSIC, Jordi Girona 18-26, 08034, Barcelona, Spain
[b] Departamento de Química Inorgánica, Instituto de Síntesis Química y Catálisis Homogénea (ISQCH), Universidad de Zaragoza-CSIC, 50009 Zaragoza, Spain

ARTICLE INFO

Dedicated to Professor Herbert Waldmann.

Keywords:
Gold
Silver
N-heterocyclic carbene
Ovarian cancer
Oxidative stress

ABSTRACT

We report four dinuclear silver(I) and gold(I) complexes containing two different bidentate *N*-heterocyclic carbene ligands (bisNHC). One of these complexes **4**, shows strong and selective anticancer activity against the human ovarian cancer cell line A2780. Mechanistically, **4** enhances the oxidative stress by stimulating reactive oxygen species production and inhibiting the scavenging activity of thioredoxin reductase. Our findings provide evidence that tuning ligand and electronic properties of metal-NHC complexes can modulate their reactivity and selectivity and it may result in potential novel anticancer drugs.

1. Introduction

Platinum-containing compounds, such as cisplatin, oxaliplatin and carboplatin, are largely used in anticancer chemotherapy. However, systemic toxicities resulting from the poor specificity and increasing development of resistances over time have significantly restricted its use and promoted the research for new anticancer drugs.[1] As a result, novel potential metal-based drugs are emerging as interesting tools as they seem to operate via different mode of action than the traditional platinum drugs, barely targeting DNA and thereby interfering with its replication and transcription.[2]

The novel antitumor metal complexes possess a great structural diversity including variations in the metal and its oxidation state (silver(I), gold(I) and (III), iridium(III), ruthenium(II)) and a variety of organic ligands including phosphines,[3] dithiocarbamates,[4] and *N*-heterocyclic carbenes (NHC).[5–6] Gold complexes, initially developed as antirheumatic agents, have dominated the research for novel anticancer drug candidates.[7]

The mechanism of action of gold complexes remains controversial. Thus, the structural variety of the active compounds suggests that the assumption of a single mode of action may not be valid. Moreover, activity may also depend on the nature and lipophilicity of the ligand, which adds further complexity to the systems. Several potential targets have been suggested including the mitochondrial pathway,[8] DNA structures,[9–10] the NRF2 transcription factor[11] and the inhibition of protein targets such as thioredoxin reductase (TrxR),[8,12] PARP-1,[13] cysteine proteases,[14] or protein tyrosine phosphatases.[15] Besides, silver complexes have been mainly investigated as anti-infective agents but their potential as cytotoxic agents against cancer cells is gaining increasing attention.[6] The mechanism of action of Ag(I) complexes is also unclear. Several targets have been identified including loss of membrane integrity due to the release of Ag(I) ions,[16] the inhibition of TrxR,[17] topoisomerase I or PARP-1.[18] Herein, four dinuclear silver(I) and gold(I) complexes containing two different bridging bidentate NHC ligands have been tested as potential anticancer agents with the aim of examining the effect of the ligands and metal centers on their biological activity. The cytotoxic effect of the compounds has been initially assessed in vitro on different cell lines, cancerous and nontumorigenic. We then evaluated their effect on TrxR inhibition and production of reactive oxygen species (ROS). Finally, the impact on cellular apoptosis and mitochondrial membrane potential was investigated in treated cells. The results obtained give a new insight into the mechanism of action of dinuclear Ag(I) and Au(I)–NHC complexes and the effect of the substitution pattern at the nitrogen atom of the *N*-heterocycle.

* Corresponding authors.
E-mail addresses: pablo.sanz@unizar.es (P.J. Sanz Miguel), gemma.triola@iqac.csic.es (G. Triola).
[1] Equal contribution.

https://doi.org/10.1016/j.bmc.2022.116814
Received 4 April 2022; Received in revised form 6 May 2022; Accepted 6 May 2022
Available online 10 May 2022

2. Materials and methods

Minimum Essential Medium Eagle (MEM), Dulbecco's modified Eagle's medium (DMEM), Roswell Park Memorial Institute medium (RPMI), fetal bovine serum (FBS), nonessential amino acids, penicillin/streptomycin, non-essential amino acids, 3-[4,5-dimethylthiazol-2-yl]-2,5-diphenyltetrazolium bromide (MTT), trypsin-EDTA, 2′,7′-dichlorofluorescin diacetate, sulforhodamine B, 5,5-dithio-bis-(2-nitrobenzoic acid) (DTNB), aprotinin, leupeptin, Tween-20, Triton X-100 and L-selenocystine were from Sigma. 4X Laemmli buffer and acrylamide were from BioRad, SDS from Fluka, and the microBCA protein assay kit from Thermo Scientific. The polyvinylidene difluoride (PVDF) membrane was from Roche. ECL Prime Western Blotting Detection Reagent was purchased from GE Healthcare. Z-VAD-FMK and E-64-D were from Enzo Life Science. Z-IEDT-FMK and Z-LEHD-FMK were from Alfa Aesar. Annexin V-FITC Early Apoptosis Detection was from Cell Signalling. The Guava EasyCyte MitoPotential Kit, Nicotinamide Adenine Dinucleotide Phosphate Hydrogen (NADPH) and sodium pyruvate were from Merck Milipore. Thioredoxin Reductase was from IMCO Corporation Ltd AB. Antibodies: TrxR was from Santa Cruz (sc-28321) and β-actin (mouse) was from Sigma (A2228). HRP secondary antibodies were from GE Healthcare.

2.1. General experimental methods

$[Au_2(bisButIm)_2](NO_3)_2$ (4) was prepared following an analogous procedure to that reported for **3**.[19] $[Ag_2(bisButIm)_2](NO_3)_2$ (**3**) (37 mg, 0.043 mmol) was reacted with [Au(tht)Cl] (27.6 mg, 0.086 mmol) in 2 mL acetonitrile at room temperature. After 16 h, AgCl was eliminated by filtration. Addition of diethylether to the filtrate provokes the precipitation of **4**, which was subsequently isolated and dried. Yield: 67 % (20 mg). ^{1}H NMR (CD_3CN, δ ppm, 300 MHz): 7.61 (s, 4H, H5im), 7.44 (s, 4H, H4im), 6.67 (dd, 4H, J_{H-H} = 259.2, 14.0, CH_2-bridge), 4.24 (dt, 8H, J_{H-H} = 6.5, 21.7; NCH_2), 2.01–1.79 (m, 8H; $CH_2CH_2CH_2$), 1.38–1.18 (m, 8H; CH_2CH_3), 0.86 (t, 12H, J_{H-H} = 7.3; CH_3). HRMS (electrospray, *m/z*): calcd. for $C_{30}H_{48}N_8Au_2$ [**4** – $(NO_3)_2$]$^{2+}$: 457.1666, found: 457.1475 (Fig. S1).

Purification of reaction products was carried out when required either by filtration or by flash chromatography using silica-gel (0.063–0.200 mm). Analytical thin layer chromatography was performed on 0.25 mm silica gel 60-F plates. ESI ionization method and mass analyzer type MicroTof-Q were used for the ESI measurements. ^{1}H NMR spectra were recorded at 300 and 400 MHz; ^{13}C NMR-APT spectra were recorded at 75 and 100 MHz; CD_3CN as the solvent. All commercially available solvents and reagents were used as received.

Cell culture. Human gastric cancer cells (HGC-27) and African green monkey kidney cells (Vero) were culture in MEM. Madin-Darby canine kidney (MDCK) cells were cultured in DMEM with 1000 mg/L of glucose. Human colorectal adenocarcinoma (HT-29) cell line was cultured in DMEM with 4500 mg/L of glucose. Humane ovary cancer (A2780) cell line was cultured in RPMI with histidine medium. All mediums were supplemented with 10% FBS and 100 ng/mL each of penicillin and streptomycin. In addition, MEM was supplemented with 1% non-essential amino acids and RPMI with 0.2% sodium pyruvate. All cell lines were cultured at 37 °C in 5% CO_2.

3-(4,5-Dimethylthiazol-2-yl)-2,5-diphenyltetrazolium bromide (MTT) assay. To determine cell viability, the colorimetric MTT metabolic activity assay was employed. Cells were seeded at a density of 0.15 × 10^6 cells/mL, 0.1 mL/well (96-well plates) and cultured at 37 °C and 5% CO_2. Twenty-four hours after seeding, cells were exposed to varying concentrations of the investigated compounds and viability was determined at the indicated times. The control culture was prepared with addition of culture medium (cell viability control) or DMSO (vehicle control) in the absence of treatment. After treatment, MTT solution (10 μL at 5 mg/mL in PBS) was added to each well and the cells were incubated for another 3 h. The solution was removed from the precipitate and the resultant formazan crystals were dissolved in DMSO (100 μL) and the absorbance intensity was measured using a microplate reader (Molecular Devices, SpectramaxM5) at 570 nm. All experiments were performed in triplicate, and the relative cell viability (%) is expressed as a percentage of cell viability relative to the cells treated with the DMSO (0.1%, vehicle group).

Sulforhodamine B assay. Initial cell viability studies with the cell lines of human ovary carcinoma (A2780, IGROV1, OVCAR3, OVCAR4, SKOV3) colon carcinoma (CACO2, COLO205, HCT116, HCT15, SW620) and hematological cells PBMC were done by OncoLead GmbH & Co. KG (München, Germany) using a SRB assay after 72 h treatment as previously described.[20] After a 48 h pre-growth period, cells were treated in triplicate with serially diluted samples of tested compounds (0.1% DMSO final concentration). The cells were allowed to grow at 37 °C for 72 h. For quantification of cell proliferation, cells were stained with fluorescent dye sulforhodamine B (SRB). Cell number that existed before treatment, at time zero, was obtained after processing cells at this time point. Calculations (GI_{50}) used nomenclature introduced by DTP NCI.[21] In SRB assays carried out in our laboratories, cells were seeded at a density of 0.1 × 10^6 cells/mL, 0.1 mL/well (96-well plates) and cultured at 37 °C and 5% CO_2. Twenty-four hours after seeding, cells were exposed to varying concentrations of tested compounds and viability was determined after the indicated times. The control culture was prepared with addition of DMSO in the absence of treatment. After 24 h, 50 μL of TCA 50% w/v and 200 μL of PBS were added to each well and the cells were incubated for 1 h at 4 °C. The solution was then removed and the plate was washed with double-distilled water. After that, 100 μL/well of SRB solution (0.4% sulforhodamine B w/v in 0.1% acetic acid) was added and the samples were incubated for another 30 min at room temperature. The plate was then washed with 1% acetic acid five times and with 200 μL of a 10 mM Tris solution (pH 10.5) were added to each well. After 30 min incubation at room temperature, the absorbance intensity was measured using a microplate reader (Molecular Devices, SpectramaxM5) at 564 nm. All experiments were performed in triplicate, and the relative cell viability (%) is expressed as a percentage of cell viability relative to the cells treated with DMSO (0.1%, vehicle group).

Inhibition of purified thioredoxin reductase (TrxR). Recombinant rat TrxR1 (ICMO Corp, Sweden; 11.2 nM) was pretreated with 100 μL potassium phosphate buffer 0.1 M pH 7.4 containing 1 mM EDTA. 0.2 mM NADPH, 0.1 mg/mL BSA at 37 °C for 30 min. Then, the compound diluted in 100 μL phosphate buffer 50 mM pH 7.4 was added and the reaction mixture was incubated for 30 min at 37 °C. After this time, DTNB in ethanol (6 mM) was added and the activity was measured by reading the absorbance at 412 nm every 20 s during 10 min. IC_{50} values were calculated using the residual activity (*vt/vo*) where *vt*, *vo* correspond to the slope of the lineal portion of the curve in the presence or absence of tested compounds.

Cellular thioredoxin reductase assay. Cells were seeded at a density of 1 × 10^6 cells/mL and cultured at 37 °C and 5% CO_2. Twenty-four hours after seeding, cells were exposed to tested compounds at the indicated times. Cells were collected with trypsin-EDTA and washed with PBS. Cell lysis was performed in 50 mM Tris-Cl (pH 7.5), 150 mM NaCl, 0.5% Triton X-100 supplemented with 2 μg/mL aprotinin, 5 μg/mL leupeptin and 1 mM PMSF. Lysates were sonicated at 4 °C for 5 s and let for 20 s on ice. This process was repeated 5 times. After 30 min on ice, samples were centrifuged for 10 min at 13.000 rpm at 4 °C and protein concentrations of the supernatants were estimated using a Micro BCA™ protein assay kit. A 45.3 mM solution of L-selenocystine and a mastermix solution (NADPH 1 mM, 3 mM L-selenocystine in $_{dd}H_2O$) were prepared following reported procedures.[22] A total reaction volume of 100 μL was assembled in clear 96-weel round bottom microplates containing 25 μL of lysates (25 μg of protein), 35 μL of buffer solution (Tris HCl 50 mM, pH 7.5, 1 mM EDTA) and 40 μL of master mix. The plate was read in 30 s intervals over an 18-min time period at 340 nm. Activity was determined by measuring the change of NADPH absorbance during the

measured time and it is reported as mol NADPH consumed/min/mg total protein.

Western blotting. Cells (200.000 cells) were plated in 6-well plates and grown for 24 h. After treatment, cells were collected with trypsin-EDTA, washed with PBS, and lysed with Laemmli sample buffer. Protein concentration was estimated by Micro BCA™ protein assay kit. Equal amounts of proteins (20 μg) were loaded and separated on a 12% polyacrylamide gel and transferred onto a PVDF membrane. Membranes were blocked with 3% BSA in TBS-T (Tris-buffered Saline containing 0.1% Tween-20) for 1 h at room temperature and incubated with anti-TrxR antibody. Alternatively, membranes were treated with 5% milk in TBS-T and incubated with anti-β-actin antibody. After washing with TBS-T, membranes were probed with the correspondent secondary antibody. Protein detection was carried out using ECL and scanning the membrane with LI-COR C-DiGit® blot scanner. Band intensity was quantified using the LI-COR Image Studio Lite software. Band intensities are expressed as a relation of the samples with the control.

ROS Detection. Oxidative metabolism was examined in triplicate samples by using 2′,7′-dichlorofluorescin diacetate. This is a non-fluorescent membrane-permeable compound which can be oxidized to 2′,7′-dichlorofluorescein in case cell has high levels of reactive oxygen species. Cells were seeded at a density of 0.1×10^6 cells/mL, 0.1 mL/well (96-well plates), cultured at 37 °C and 5% CO_2 and allowed to adhere for 24 h. Then 2′,7′-dichlorofluorescin diacetate (25 μM) in DMSO was added and after 1 h, compounds (or DMSO as a vehicle) were then added and cells were incubated 3 h. If required, scavengers (Trolox (50 μM) or sodium pyruvate (10 mM)) were added together with tested compounds. Fluorescence was measured by a microplate reader (Molecular Devices, SpectramaxM5) at an excitation wavelength of 485 nm and emission wavelength of 538 nm. ROS levels were normalized to SRB values as an indicator of cellular protein amount.

Apoptosis. Cells were seeded in 6 well plates (0.15×10^6 cells per mL), cultured at 37 °C and 5% CO_2 and allowed to adhere for 24 h. Then, cells were treated for 24 h with either Auranofin, **4** or DMSO (control) at the specified concentrations. When required, caspase inhibitors (Z-VAD-FMK, Z-IETD-FMK, Z-LEHD-FMK (20 μM)) were added 1 h before treatment with the compounds. After treatments, cells were collected by trypsinization, washed twice with PBS and centrifuged (200 rpm/3 min). The Annexin V-FITC Early Apoptosis Detection Kit was used to analyze cell apoptosis according to manufacturer's instructions. Briefly, the cell pellet was resuspended in 96 μL of Annexin V binding buffer, 1 μL of FITC-Annexin V and 12.5 μL of propidium iodide. After 10 min on ice in the dark, apoptosis was determined using a Guava easyCyte™ flow cytometer (Merck Millipore). Samples were excited at 488 nm with barrier filters and FITC and PI emissions were detected with 525 nm and 575 nm filters, respectively. Data were analyzed by InCyte Software and plotted for Annexin V-FITC and PI in a two-way dot plot. Results are shown as a percentage of cells.

2.2. Mitochondrial membrane potential

Cells were seeded in 6 well plates (0.1×10^6 cells per mL), cultured at 37 °C and 5% CO_2, and allowed to adhere for 24 h. Cells were then treated for 24 h with either Auranofin as a positive control, **4** or DMSO (control) at the specified concentrations. After treatments, cells were collected by trypsinization, washed twice with PBS containing 5% BSA and centrifuged (200 rpm/3 min). Cell pellet was then resuspended in 200 μL medium and seeded into a 96-well plate (1 sample / well). 4 μL of a previously prepared 50X solution of JC-1 and 7-AAD (7-amino-actinomycin) were added to each well and cells were incubated for 30 min at 37 °C and 5% CO_2. Finally, cells were collected and mitochondrial membrane potential was measured using a Guava easyCyte™ flow cytometer (Merck Millipore). The percentage of cells of green (530 nm) and red (590 nm) fluorescence of JC-1 was analyzed.

3. Results and discussion

3.1. Synthesis

Dinuclear silver $[Ag_2(bisNHC)_2]^{2+}$ cations (Chart 1) have been prepared with slight modifications of reported methods: $[Ag_2(bisMeOEtIm)_2](NO_3)_2$ (**1**)[23] (bisMeOEtIm = bis(2-methoxyethyl-1-imidazole) methane), and $[Ag_2(bisButIm)_2](NO_3)_2$ (**2**)[19] (bisButIm = bis(*n*-butlyl-1-imidazole)methane). Subsequent treatment of **1** and **2** with [Au(tht)Cl] (tht = tetrahydrothiophene) under mild conditions resulted in the respective gold $[Ag_2(bisNHC)_2]^{2+}$ cations, namely, $[Au_2(bisMeOEtIm)_2](NO_3)_2$ (**3**)[24] and $[Au_2(bisButIm)_2](NO_3)_2$ (**4**). In addition to the metal exchange, the structural difference of these compounds lies in the formal substitution of an ether group (–O–) by a methylene ($–CH_2–$) entity. As a result, it is interesting to point out that solubility of the ether compounds (**1** and **3**) is significantly higher in water if compared to the *n*-butyl derivatives (**2** and **4**). All the complexes were stable under physiological conditions to perform all the studies described in this work.

3.2. Cytotoxicity

The in vitro cytotoxicity of the complexes **1**–**4** was initially assessed using a 3-(4,5-dimethylthiazol-2-yl)-2,5-diphenyltetrazolium bromide (MTT) assay and different cell lines, the human gastric cancer cell line HGC-27 and the non-tumorigenic Madin-Darby Canine Kidney Epithelial (MDCK) cell line. Half maximal inhibitory concentrations (IC_{50}) were measured after 24 h treatment and the results are summarized in Table 1. A dose-dependent inhibition of cell growth was observed for all the metal complexes $[M_2(bisNHC)_2]^{2+}$ except for Au(I)–NHC **3**, whereas **4**, only differing from **3** by the nature of the ligand showed an increased potency for the cancerous cell line HGC-27, that was confirmed after longer treatments (72 h exposure). Contrarily, both Ag(I)-containing compounds **1** and **2** showed higher cytotoxicity and similar IC_{50} in all the cases.

Afterwards, the triggering of the antiproliferative effects of the most effective and selective complex **4** was further evaluated on a panel of cancer cell lines, including five human ovarian carcinoma cell lines (A2780, IGROV1, OVCAR3, OVCAR4, SKOV3) and six human colon carcinoma cell lines (CACO2, COLO205, HCT116, HCT15, SW620, HT-29), as well as the non-cancer African green monkey kidney (Vero) and the resting, non-proliferative peripheral blood mononuclear cells (PBMC). In this case, cell viability was measured after 72 h exposure using the Sulforhodamine B (SRB) assay, which quantifies the total amount of cellular protein and it is independent of mitochondrial activity. The results of the panel screening proved outstanding antiproliferative potencies of **4** (GI_{50}, the concentration causing 50% cell growth inhibition in relation to the initial cell seeding number, of 0.63 μM) towards the ovarian cancer cell line A2780. Moderate potencies were also observed in other cells lines with mean GI_{50} data in the range of 5–15 μM. No activity could be observed in in the human ovarian carcinoma cells OVCAR4 and SKOV3 or in quiescent PMBC suggesting that antiproliferative activities are related to actively cycling cells (Table 2). The silver complex **2** (IC_{50} 0.43 μM) displayed similar potency in A2780 cells, whereas the gold complex **3** was again not toxic at the concentrations tested.

3.3. TrxR inhibition

The selenoenzyme thioredoxin reductase (TrxR) has already been identified as cellular target for gold[25] and silver complexes.[17,26] TrxR plays a major role in the regulation of the intracellular redox homeostasis. It is required to convert oxidized thioredoxin (Trx) into its reductive form, which can scavenge ROS and consequently improves cell viability under oxidative stress.[27] Moreover, TrxR variants appear to be overexpressed in certain types of cancer[28] and its inhibition increases sensitivity to oxidants and leads to apoptosis.[29]

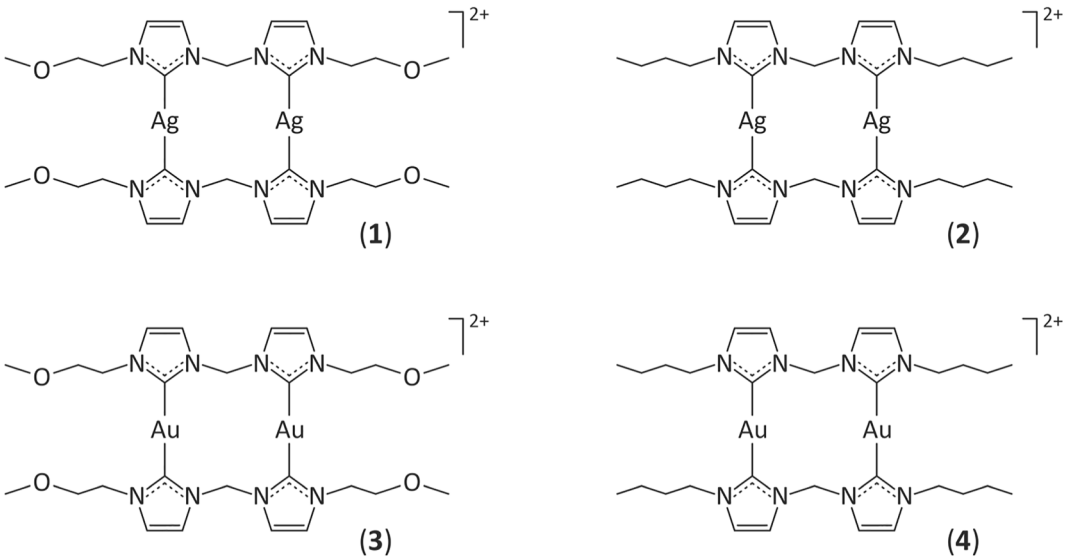

Chart 1.

Table 1
Antiproliferative effects of $[Ag_2(bisNHC)_2]^{2+}$ **1**–**2** and $[Au_2(bisNHC)_2]^{2}$ **3**–**4** expressed as IC_{50} values (μM, (95% confidence intervals)); N.A.: not active.

Cell line	IC_{50} (μM)				
$[M_2(bisNHC)_2]^{2+}$	**1**	**2**	**3**	**4**	
Time (h)	24	24	24	24	72
HGC-27	11.4 (10.4–12.4)	11.8 (10.4–13.4)	N.A.	48.7 (37.6–63.2)	3.45 (3.2–3.7)
MDCK	4.8 (4.3–5.3)	3.0 (2.0–4.6)	N.A.	89.0 (61.0–130.0)	54.67 (45.7–65.2)

Table 2
Antiproliferative effects of $[Au_2(bisNHC)_2]^{2}$ **4** expressed as GI_{50} values (μM, 95% confidence intervals); N.A. not active.

Cell line	GI_{50} (μM)
A2780	0.63 (0.16–2.5)
IGROV1	9.62 (2.5–36,99)
OVCAR3	5.32 (1.13–25.0)
OVCAR4	N.A.
SKOV3	N.A.
CACO2	4.99 (0.99–25.0)
COLO205	7.44 (2.21–25.0)
HCT116	6.44 (1.67–25.0)
HCT15	9.85 (2.5–38.88)
SW620	6.82 (1.85–25.0)
HT-29	15.21 (13.3–17.0)
Vero	12.59 (10.98–14.45)
PBMC	N.A.

Whereas direct targeting of TrxR by Au(I)–NHC compounds have been widely investigated, its inhibition by Ag(I)-based complexes remains less characterized and no evidences of TrxR inhibition by dinuclear $[Ag_2(bisNHC)_2]^{2+}$ complexes have been reported so far. Hence, we next evaluated whether the antiproliferative effects of the $[Ag_2(bisNHC)_2]^{2+}$ and $[Au_2(bisNHC)_2]^{2+}$ complexes could be explained by direct inhibition of TrxR. Thus, the inhibitory effect of the Ag(I)-based complex **2** and the two Au(I) complexes **3** and **4** was next studied on mammalian TrxR. Enzyme activity was efficiently inhibited by all three complexes. However, whereas **2** and **4** exhibited IC_{50} values in the low nanomolar range (8.9 and 4.8 nM), the activity of the noncytotoxic **3**, only differing from **4** by the aliphatic chain linked to the imidazole moiety, dropped to 13.5 μM (Supporting Information Fig. S2). Although these results suggest a possible correlation between cell viability and TrxR inhibition, it was still unclear whether the selectivity profile observed for **4** can be solely explained based on TrxR activity.

The rapid proliferation of cancer cells requires high metabolic activity. To compensate this high oxidative stress, the expression and activity of TrxR is upregulated in several tumor types.[30] As a result, cancer cells may have an increased dependency on TrxR activity, what makes them more vulnerable to the effect of small molecules targeting this enzyme. To investigate this hypothesis, we measured the protein levels of TrxR1 in A2780 cells compared to the non-cancer cells Vero and the less sensitive HT-29. Immunoblot analysis of TrxR1 relative abundance showed that contrarily to what may have been expected, Vero and HT-29 cells showed increased levels of the enzyme as compared with A2780 cells (Fig. 1B). Next, enzyme activity was measured using a continuous direct assay based on the reduction of L-Selenocystine and cell lysates as a source of enzyme.[22] In line with the previous results, TrxR activity was slightly increased in HT-29 and Vero cells compared with A2780 cells (Fig. 1C, Supporting Information Fig. S3). These results suggested that the larger vulnerability of A2780 cells could not only rely on an increased activity of TrxR.

3.4. Reactive oxygen species

The higher metabolic activity of cancer cells is usually associated

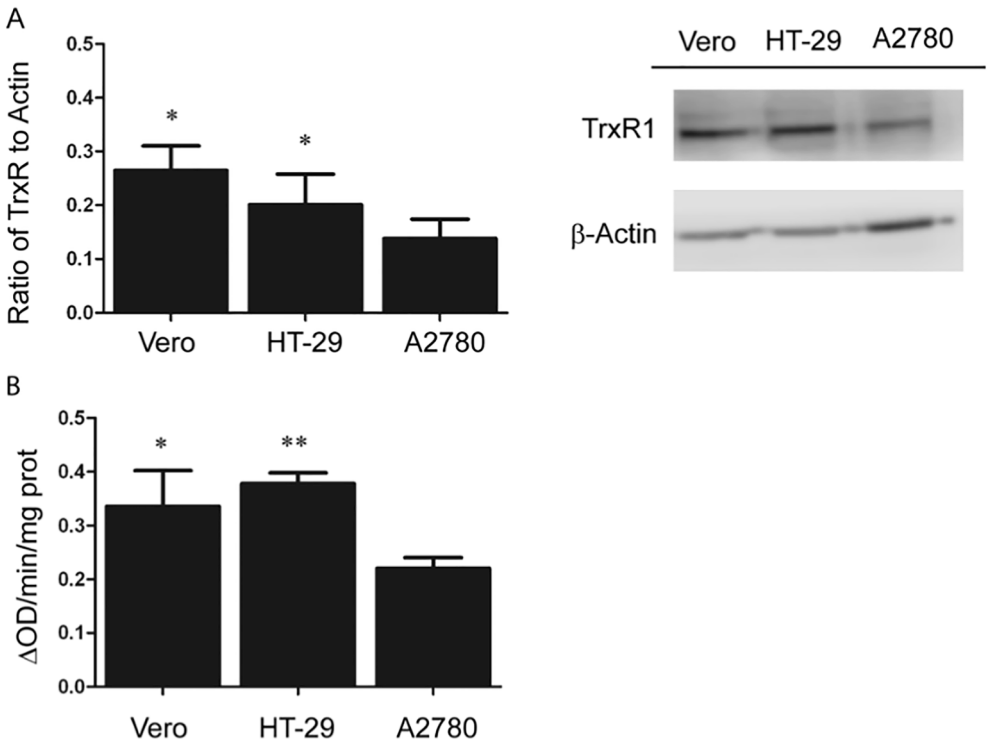

Fig. 1. A) TrxR protein expression in Vero, HT-29 and A2780 cells. Densitometry of immunoblot signals normalized to actin expression. Bar chart shows quantification of protein levels compared to actin control as a loading control. One representative blot is shown of two independent experiments. B) TrxR activity measured in the indicated cell lysates using L-Selenocystine as a substrate and a continuous direct assay (Error bars show Mean ± SD, *P < 0.05; ** P < 0.01; Student's test).

with the generation of abundant ROS, such as superoxide anion, hydrogen peroxide, singlet oxygen or hydroxyl radical. As an excessive ROS can be toxic, cancer cells are likely to be more vulnerable to damage by further oxidative insults and this altered redox status can be exploited for therapeutic benefits.[31] Thus, an increase of ROS above certain threshold levels, induced by either inhibiting ROS scavenging or enhancing ROS production, should lead to selective death of malignant cells sparing normal cells.

The thioredoxin system maintains the intracellular redox homeostasis by directly scavenging ROS. However, as TrxR inhibition seems no to be the solely responsible of the observed effect, we decided to investigate if basal intracellular ROS levels could contribute to the selective toxicity observed in A2780 cells. A fluorogenic probe, 2′,7′-dichlorofluorescin diacetate (DCFH-DA) was employed, which in the presence of intracellular ROS is converted to highly fluorescent dichlorofluorescein (DCF). As shown in Fig. 2A, the results indicated that the ovarian cancer cell line A2780 presents higher baseline levels of ROS as compared to the less-sensitive Vero and HT-29 cell lines.

Gold compounds have been described to markedly increase the production of intracellular ROS.[32] An increase could specifically affect A2780 cells, that may be more vulnerable to further oxidative stress due to their high basal levels of ROS, probably closer to cell-death threshold. To test this hypothesis, we next investigated the effect of complexes **2** and **4** on the intracellular ROS production. Indeed, a significant ROS accumulation was observed in cells treated with both metal NHC complexes cases. Hence, treatment with **4** resulted in a 3-, 2- and 2.5-fold increase in DCF fluorescence signals in Vero, HT-29 and A2780 cells respectively, whereas treatment with **2** resulted in a marked 4, 5.2 and 5.4-fold increase as compared with the vehicle treated cells (Fig. 2A).

To explore whether ROS production is required for the cell death induced by **4**, Vero cells were treated with **4** in the presence of the hydrogen peroxide scavenger sodium pyuvate[33] or 6-hydroxy-2,5,7,8-tetramethylchromane-2-carboxylic acid (trolox), a water-soluble derivative of vitamin E and a scavenger of peroxyl and alkoxyl radicals.[34] The results showed that trolox and sodium pyruvate almost completely suppressed ROS accumulation induced by **4** (Fig. 2B). We next examined the possible relationship between ROS overproduction and decreased cell viability. Indeed, treatment with trolox and sodium pyruvate scavengers partially inhibited cell death induced by **4** and neutralized its anti-proliferative effect (Fig. 2C). Taken all together, these results indicate that increased ROS levels play a key role in **4**-elicited cell death.

3.5. Apoptosis assay

It is well established that the generation of ROS can cause cell death by either apoptosis or necrosis. Hence, to explore the cell death caused by **4** and to determine the most prevalent death mechanism, an apoptosis assay was next carried out in A2780 cells. To this end, A2780 cells were treated with vehicle alone as control or with three different concentrations of **4**. The established gold-containing drug Auranofin was included as a positive control. This gold containing compound is clinically used to treat rheumatic arthritis but has been shown to induce apoptosis in several cancer cell lines.[35] After Annexin V-FITC/PI staining, cells were a subsequently analyzed cells by flow cytometry.[36] As shown in Fig. 3, the cell-state distribution after treatment indicated that apoptosis was the main cell death mechanism as in cells treated with 2.5 μM 5 μM and 10 μM, the total percentage of early and late apoptotic cells were 29.4%, 34.5% and 49.2 % respectively. In contrast, only 5.5% of apoptotic cells were detected in the vehicle-treated cells (Fig. 3A, B).

To elucidate whether apoptosis was triggered through caspase-dependent or independent mechanisms, we explored the activation of caspases. Thus, pretreatment of cells with the pan-caspase inhibitor Z-VAD-FMK (20 μM) for 1 h partially prevented **4**-induced cell death (20% vs 39%), thus suggesting that a caspase-dependent mechanism may be involved. Next, the involvement of the extrinsic or the intrinsic signalling pathway in apoptosis induction was investigated. The extrinsic signalling pathway involves death receptors located at the membrane, the transmission of the signal to intracellular pathways and the

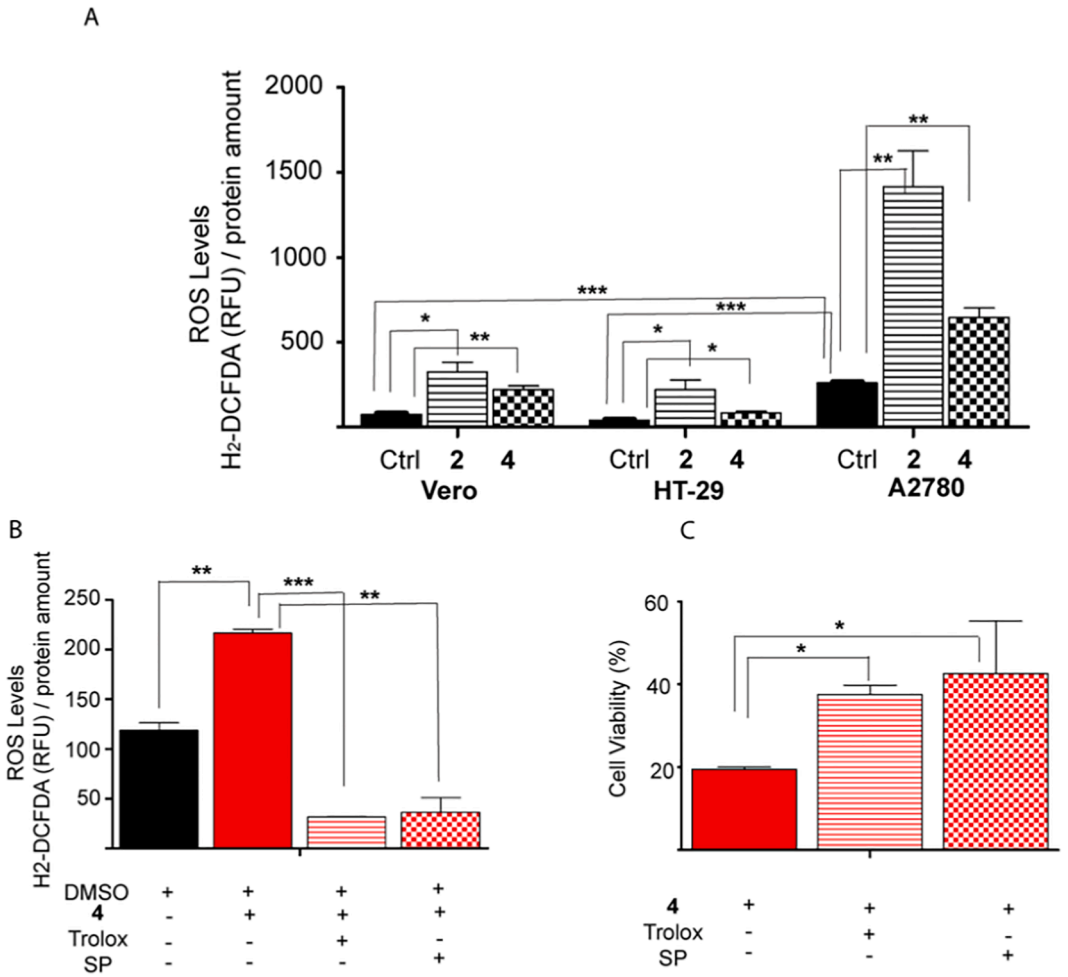

Fig. 2. The production of ROS was monitored after 4 h treatment of cells with **2** or **4** (9 μM) or vehicle (DMSO) by fluorescence of dichlorofluorescein. ROS levels were normalized to SRB values as an indicator of cellular protein amount. B) Antioxidant effects on **4**-induced toxicity. ROS production was monitored in Vero cells treated for 4 h with Trolox or sodium pyruvate (SP) in presence of **4** (13 μM). C) Viability of Vero cells was determined by an SRB assay after 24 h treatment. Data are the mean ± SD of three experiments (*P < 0.05; ** P < 0.01; ***P < 0.001; Student's test).

implication of caspase-8. The intrinsic pathway may be caused by different stimuli including ischemia and oxidative stress and involves the activation of caspase-9. To this end, cells were pretreated with a caspase-8 (Z-IETD-FMK, extrinsic pathway) or a caspase-9 (Z-LEHD-FMK, intrinsic pathway) inhibitor. Interestingly, the percentage of apoptotic cells markedly decreased upon treatment with the caspase-9 inhibitor Z-LEHD-FMK (39% vs 12%), whereas no changes could be observed in cells treated with caspase-8 inhibitor, thus suggesting the implication of the mitochondrial pathway (Supporting Information Fig. S4).

3.6. Mitochondria permeabilization

The apoptosis data suggested the existence of mitochondria damage that correlate well with the previously observed increase of ROS levels, as mitochondria are the main source of intracellular ROS production. In addition, changes in mitochondrial membrane potential (MMP, $\Delta\Psi_m$) and loss of membrane permeability can be an indicator of impaired mitochondrial integrity and the activation of the intrinsic apoptotic pathway. Therefore, the effects of **4** on MMP were next investigated by employing 5,5′,6,6′-tetrachloro-1,1′,3,3′-tetraethylbenzimidazolcarbocyanine iodide (JC-1), a cationic dye that inserts into the mitochondrial membrane forming yellow aggregates. When MMP collapses, JC-1 diffuses to the cytosol forming monomers with green emission.[37] Therefore, JC-1 has been widely used to detect mitochondrial depolarization. As it can be seen in Fig. 3C and S5, analysis of MMP by JC-1 labeling revealed that the percentage of depolarized cells significantly increased in A2780 cells after treatment with **4**. This effect was dose-dependent clearly indicating that **4** induces $\Delta\Psi_m$ changes in A2780 cells. As the dissipation of MMP is considered to be a mitochondrial disruption event during apoptosis, these results are in alignment with the implication of the intrinsic pathway in the **4**-mediated cell death.

4. Conclusions

Ovarian cancer is the most lethal gynecologic malignancy. Current standard treatment consists of surgery and chemotherapy with cisplatin and derivatives, either alone or in combination with other drugs. However, chemotherapy resistance leading to recurrent disease has emerged as a major challenge in ovarian cancer. Therefore, the development of additional therapeutic approaches, ideally acting on different mechanisms of action, has emerged as a promising approach for cancer therapy. Herein, we describe series of novel dinuclear gold and silver complexes featuring two different bridging bis(NHC) ligands. The compounds have been tested for their antiproliferative effects on a variety of cancerous and nontumorigenic cells lines. The results are indicative of a role of both the metallic center and the functionalized ligand in the biological activity.[38] Hence, the $[Au_2(bisNHC)_2]^{2+}$ complex **4** bearing a *n*-butyl group on the nitrogen of the imidazole rings display promising activity with significant selectivity towards the

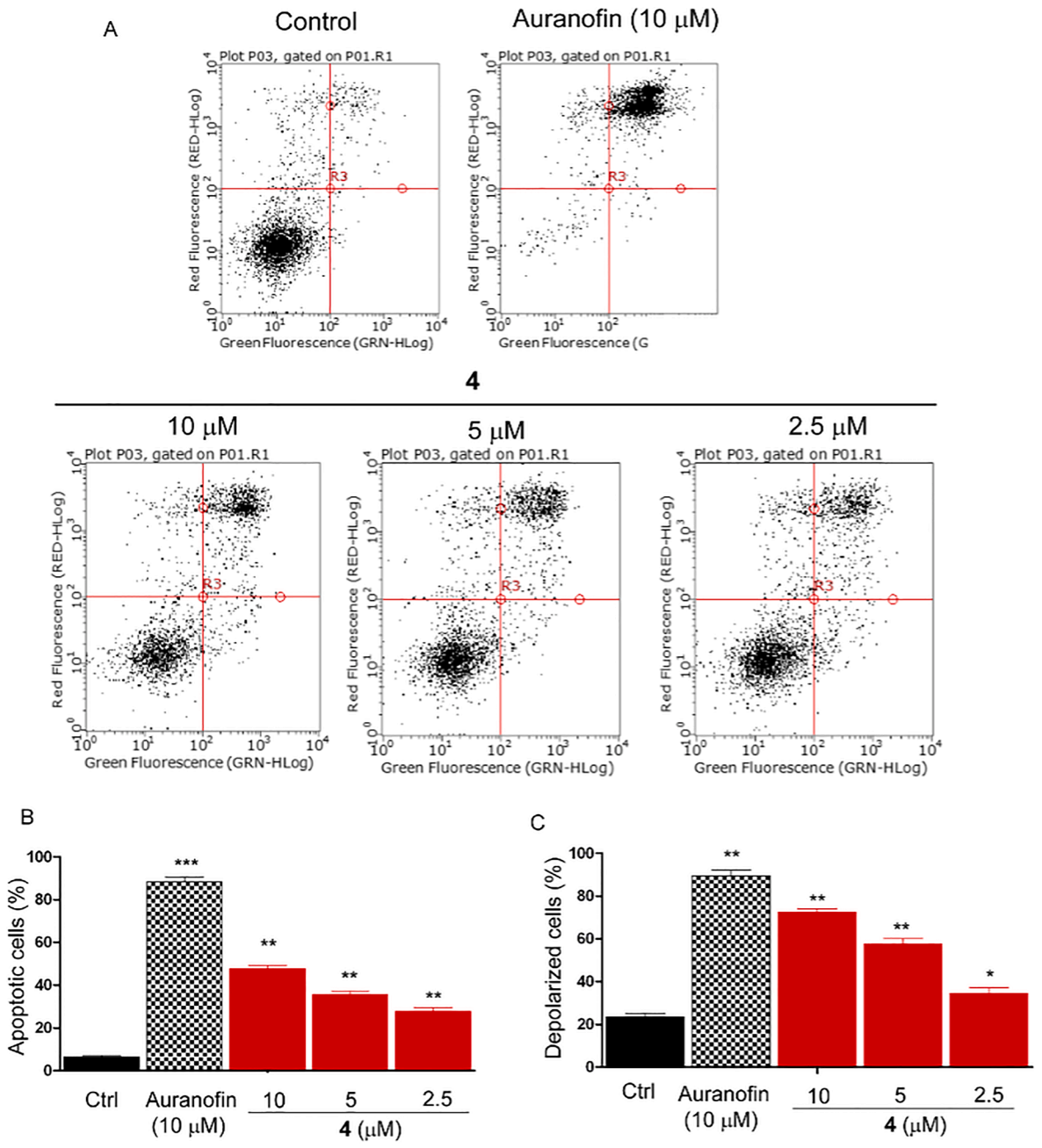

Fig. 3. Cell apoptosis was analyzed in A2780 cells by flow cytometry using Annexin V-FITC/PI double staining. A) Representative cell distribution plots. B) Percentage of apoptotic cells. C) Assessment of changes in mitochondrial membrane potential in response to Auranofin and **4**. Mitochondrial depolarization was monitored in A2780 cells using the membrane permeable dye JC-1. Each value represents the mean ± SD of two experiments (*P < 0.05; ** P < 0.01; ***P < 0.001; Student's test).

human ovarian cancer cell line A2780, whereas the 2-methoxy ethyl-substituted **3** is ineffective in all the cell lines tested. Lipophilicity has been previously shown to play a role in the selective toxicity of cationic Au(I) complexes to cancer cells over noncancer cells, probably due to selective accumulation in tumor cell mitochondria.[8] Notably, the replacement of the gold with silver results in a superior and general toxicity leading to detriment of the selectivity, irrespective of the substitution pattern of the imidazole moiety. One of the possible reasons is that Ag(I)–NHC complexes present an increased lability compared with Au(I) complexes resulting in a faster release of Ag^{+} ions. Higher cytotoxicity and increase in ROS levels for silver complexes have been also previously described as compared with gold analogues, leading to the detriment of the selectivity towards cancer cells.[39]

Treatment with the $[Au_2(bisNHC)_2]^{2+}$ complex **4** resulted in a substantial alteration of the cellular redox homeostasis mediated by the combined effect of TrxR inhibition and enhanced ROS production. This oxidative stress ultimately results in the depolarization of mitochondrial membrane and the death of the treated cells via caspase-9 dependent apoptosis, whereas treatment with ROS scavengers can rescued cells from damage. The high basal ROS levels detected in A2780 may have a significant effect on their capacity to cope with oxidative stress and make them more vulnerable to damage caused by further elevation of ROS. Taken together, those data suggest that the $[Au_2(bisNHC)_2]^{2+}$ complex **4** could be a promising drug candidate for cancer therapy.

Declaration of Competing Interest

The authors declare that they have no known competing financial interests or personal relationships that could have appeared to influence the work reported in this paper.

Acknowledgements

We acknowledge financial support from Ministerio de Ciencia e Innovación, Spain (RTI2018-096323-B-I00), the Marie Curie Career Integration Grants (PCIG12-GA-2012-33835), the Max Planck Society (MPG Partner Group), the Aragon Government (E42_20R) and the University of Zaragoza.

Appendix A. Supplementary material

Supplementary data to this article can be found online at https://doi.org/10.1016/j.bmc.2022.116814.

References

1 Kelland L. The resurgence of platinum-based cancer chemotherapy. *Nat Rev Cancer*. 2007;7(8):573–584. https://doi.org/10.1038/nrc2167.
2 Lazarevic T, Rilak A, Bugarcic ZD. Platinum, palladium, gold and ruthenium complexes as anticancer agents: current clinical uses, cytotoxicity studies and future perspectives. *Eur J Med Chem*. 2017;142:8–31. https://doi.org/10.1016/j.ejmech.2017.04.007.
3 Schuh E, Valiahdi SM, Jakupec MA, Keppler BK, Chiba P, Mohr F. Synthesis and biological studies of some gold(I) complexes containing functionalised alkynes. *Dalton Trans*. 2009;48:10841–10845. https://doi.org/10.1039/b911234k.
4 Marzano C, Ronconi L, Chiara F, et al. Gold(III)-dithiocarbamato anticancer agents: activity, toxicology and histopathological studies in rodents. *Int J Cancer*. 2011;129(2):487–496. https://doi.org/10.1002/ijc.25684.
5 Zou T, Lum CT, Lok CN, Zhang JJ, Che CM. Chemical biology of anticancer gold(III) and gold(I) complexes. *Chem Soc Rev*. 2015;44(24):8786–8801. https://doi.org/10.1039/c5cs00132c.
6 Johnson NA, Southerland MR, Youngs WJ. Recent developments in the medicinal applications of silver-NHC complexes and imidazolium salts. *Molecules*. 2017;22(8):1263. https://doi.org/10.3390/molecules22081263.
7 Oehninger L, Rubbiani R, Ott I. N-heterocyclic carbene metal complexes in medicinal chemistry. *Dalton Trans*. 2013;42(10):3269–3284. https://doi.org/10.1039/c2dt32617e.
8 Hickey JL, Ruhayel RA, Barnard PJ, Baker MV, Berners-Price SJ, Filipovska A. Mitochondria-targeted chemotherapeutics: the rational design of gold(I) N-heterocyclic carbene complexes that are selectively toxic to cancer cells and target protein selenols in preference to thiols. *J Am Chem Soc*. 2008;130(38):12570–12571. https://doi.org/10.1021/ja804027j.
9 Bertrand B, Stefan L, Pirrotta M, et al. Caffeine-based gold(I) N-heterocyclic carbenes as possible anticancer agents: synthesis and biological properties. *Inorg Chem*. 2014;53(4):2296–2303. https://doi.org/10.1021/ic403011h.
10 Wragg D, de Almeida A, Bonsignore R, Kuhn FE, Leoni S, Casini A. On the mechanism of gold/NHC compounds binding to DNA G-quadruplexes: combined metadynamics and biophysical methods. *Angew Chem Int Ed*. 2018;57(44):14524–14528. https://doi.org/10.1002/anie.201805727.
11 Zhang C, Fortin P, Barnoin G, et al. An artemisinin-derivative–(NHC)gold(I) hybrid with enhanced cytotoxicity through inhibition of NRF2 transcriptional activity. *Angew Chem Int Ed*. 2020;59(29):12062–12068. https://doi.org/10.1002/ange.202002992.
12 Zou T, Lum CT, Lok CN, To WP, Low KH, Che CM. A Binuclear gold(I) complex with mixed bridging diphosphine and bis(N-heterocyclic carbene) ligands shows favorable thiol reactivity and inhibits tumor growth and angiogenesis in vivo. *Angew Chem Int Ed*. 2014;53(23):5810–5814. https://doi.org/10.1002/anie.201400142.
13 Mendes F, Groessl M, Nazarov AA, et al. Metal-based inhibition of poly(ADP-ribose) polymerase–the guardian angel of DNA. *J Med Chem*. 2011;54(7):2196–2206. https://doi.org/10.1021/jm2000135.
14 Fricker SP. Cysteine proteases as targets for metal-based drugs. *Metallomics*. 2010;2(6):366–377. https://doi.org/10.1039/b924677k.
15 Krishnamurthy D, Karver MR, Fiorillo E, et al. Gold(I)-mediated inhibition of protein tyrosine phosphatases: a detailed in vitro and cellular study. *J Med Chem*. 2008;51(15):4790–4795. https://doi.org/10.1021/jm800101w.
16 Hartinger CG, Dyson PJ. Bioorganometallic chemistry–from teaching paradigms to medicinal applications. *Chem Soc Rev*. 2009;38(2):391–401. https://doi.org/10.1039/b707077m.
17 Citta A, Schuh E, Mohr F, et al. Fluorescent silver(I) and gold(I)-N-heterocyclic carbene complexes with cytotoxic properties: mechanistic insights. *Metallomics*. 2013;5(8):1006–1015. https://doi.org/10.1039/c3mt20260g.
18 Allison SJ, Sadiq M, Baronou E, et al. Preclinical anti-cancer activity and multiple mechanisms of action of a cationic silver complex bearing N-heterocyclic carbene ligands. *Cancer Lett*. 2017;403:98–107. https://doi.org/10.1016/j.canlet.2017.04.041.
19 Cebollada A, Vellé A, Iglesias M, et al. Direct X-ray scattering evidence for metal-metal interactions in solution at the molecular level. *Angew Chem Int Ed*. 2015;54(43):12762–12766. https://doi.org/10.1002/anie.201505736.
20 Prinz H, Ridder AK, Vogel K, et al. N-heterocyclic (4-phenylpiperazin-1-Yl) methanones derived from phenoxazine and phenothiazine as highly potent inhibitors of tubulin polymerization. *J Med Chem*. 2017;60(2):749–766. https://doi.org/10.1021/acs.jmedchem.6b01591.
21 Paull KD, Shoemaker RH, Hodes L, et al. Display and analysis of patterns of differential activity of drugs against human tumor cell lines: development of mean graph and COMPARE algorithm. *J Natl Cancer Inst*. 1989;81(14):1088–1092. https://doi.org/10.1093/jnci/81.14.1088.
22 Cunniff B, Snider GW, Fredette N, Hondal RJ, Heintz NH. A Direct and continuous assay for the determination of thioredoxin reductase activity in cell lysates. *Anal Biochem*. 2013;443(1):34–40. https://doi.org/10.1016/j.ab.2013.08.013.
23 Vellé A, Cebollada A, Iglesias M, Sanz Miguel PJ. Argentophilicity as essential driving force for a dynamic cation-cation host-guest system: $[Ag(acetonitrile)_2]^+ \subset [Ag_2(Bis\text{-}NHC)_2]^{2+}$ (NHC = N-heterocyclic carbene). *Inorg Chem*. 2014;53(19):10654–10659. https://doi.org/10.1021/ic501715h.
24 Vellé A, Rodríguez-Santiago L, Sodupe M, Sanz Miguel PJ. Enhanced metallophilicity in metal-carbene systems: stronger character of aurophilic interactions in solution. *Chem Eur J*. 2020;26(5):997–1002. https://doi.org/10.1002/chem.201904507.
25 Gromer S, Arscott LD, Williams Jr CH, Schirmer RH, Becker K. Human placenta thioredoxin reductase. isolation of the selenoenzyme, steady state kinetics, and inhibition by therapeutic gold compounds. *J Biol Chem*. 1998;273(32):20096–20101.
26 Pellei M, Gandin V, Marinelli M, et al. Synthesis and biological activity of ester- and amide-functionalized imidazolium salts and related water-soluble coinage metal N-heterocyclic carbene complexes. *Inorg Chem*. 2012;51(18):9873–9882. https://doi.org/10.1021/ic3013188.
27 Tanaka T, Hosoi F, Yamaguchi-Iwai Y, et al. Thioredoxin-2 (TRX-2) is an essential gene regulating mitochondria-dependent apoptosis. *EMBO J*. 2002;21(7):1695–1703. https://doi.org/10.1093/emboj/21.7.1695.
28 Berggren M, Gallegos A, Gasdaska JR, Gasdaska PY, Warneke J, Powis G. Thioredoxin and thioredoxin reductase gene expression in human tumors and cell lines, and the effects of serum stimulation and hypoxia. *Anticancer Res*. 1996;16(6B):3459–3466.
29 Chen Y, Cai J, Jones DP. Mitochondrial thioredoxin in regulation of oxidant-induced cell death. *FEBS Lett*. 2006;580(28–29):6596–6602. https://doi.org/10.1016/j.febslet.2006.11.007.
30 Lincoln DT, Ali Emadi EM, Tonissen KF, Clarke FM. The thioredoxin-thioredoxin reductase system: over-expression in human cancer. *Anticancer Res*. 2003;23(3B):2425–2433.
31 Trachootham D, Alexandre J, Huang P. Targeting cancer cells by ROS-mediated mechanisms: a radical therapeutic approach? *Nat Rev Drug Discov*. 2009;8(7):579–591. https://doi.org/10.1038/nrd2803.
32 Wang Y, He QY, Sun RW, Che CM, Chiu JF. GoldIII porphyrin 1a induced apoptosis by mitochondrial death pathways related to reactive oxygen species. *Cancer Res*. 2005;65(24):11553–11564. https://doi.org/10.1158/0008-5472.CAN-05-2867.
33 Kladna A, Marchlewicz M, Piechowska T, Kruk I, Aboul-Enein HY. Reactivity of pyruvic acid and its derivatives towards reactive oxygen species. *Luminescence*. 2015;30(7):1153–1158. https://doi.org/10.1002/bio.2879.
34 Huang D, Ou B, Prior RL. The chemistry behind antioxidant capacity assays. *J Agric Food Chem*. 2005;53(6):1841–1856. https://doi.org/10.1021/jf030723c.
35 Zou P, Chen M, Ji J, et al. Auranofin induces apoptosis by ROS-mediated ER stress and mitochondrial dysfunction and displayed synergistic lethality with piperlongumine in gastric cancer. *Oncotarget*. 2015;6(34):36505–36521. https://doi.org/10.18632/oncotarget.5364.
36 Liu G, Lynch JK, Freeman J, et al. Discovery of potent, selective, orally bioavailable stearoyl-CoA desaturase 1 inhibitors. *J Med Chem*. 2007;50(13):3086–3100. https://doi.org/10.1021/jm070219p.
37 Ly JD, Grubb DR, Lawen A. The mitochondrial membrane potential (deltapsi(m)) in apoptosis; an update. *Apoptosis*. 2003;8(2):115–128.
38 Rubbiani R, Schuh E, Meyer A, et al. TrxR inhibition and antiproliferative activities of structurally diverse gold N-heterocyclic carbene complexes. *MedChemComm*. 2013;4:942–948. https://doi.org/10.1039/C3MD00076A.
39 Guarra F, Busto N, Guerri A, et al. Cytotoxic Ag(I) and Au(I) NHC-carbenes bind DNA and show TrxR inhibition. *J Inorg Biochem*. 2020;205, 110998. https://doi.org/10.1016/J.JINORGBIO.2020.110998.